V European Conference on Computational Fluid Dynamics
ECCOMAS CFD 2010
J. C. F. Pereira and A. Sequeira (Eds)
Lisbon, Portugal,14-17 June 2010

ROBUST MULTIGRID SOLUTION OF RANS EQUATIONS WITH TWO-EQUATION TURBULENCE MODELS

Mark Wasserman[*], Yair Mor-Yossef[†], Irad Yavneh[◇] and J. Barry Greenberg[◇]

[*,◇] Technion, Israel Institute of Technology
Haifa 32000, Israel
e-mail: markw@tx.technion.ac.il

[†]Israeli CFD Center
Caesarea Industrial Park 38900, Israel
e-mail: yairm@iscfdc.co.il

Key words: RANS, turbulence models, positivity preservation, numerical stiffness, source term, multigrid

Abstract. *The design of a new, truly robust multigrid framework for the solution of steady-state Reynolds-averaged Navier-Stokes (RANS) equations with two-equation turbulence models is presented. While the mean-flow equations and the turbulence model equations are advanced in time in a loosely-coupled manner, their multigrid cycling is strongly coupled (FC-MG). Thanks to the loosely-coupled approach, the unconditionally positive-convergent implicit time integration scheme for two-equation turbulence models (UPC) is used. An extension of the UPC scheme within the multigrid method is proposed. The resulting novel FC-MG-UPC algorithm is nearly free of artificial stabilizing techniques, leading to increased multigrid efficiency. To demonstrate the robustness of the proposed algorithm, it is applied to linear and non-linear two-equation turbulence models. Numerical experiments are conducted, simulating separated flow about the NACA4412 airfoil and transonic flow about the RAE2822 airfoil. Results obtained from numerical simulations demonstrate the strong consistency and case-independence of the method.*

1 INTRODUCTION

Turbulent flow simulations employing the Reynolds-Averaged Navier-Stokes (RANS) equations are widely used in research, development, and design processes. Among the RANS turbulence models, the two-equation k-ω [1] and k-ϵ [2] closure models are most widely used since they are considered well-balanced in terms of computational requirements and physical rationale. Two-equation RANS turbulence models are based on transport equations for turbulence quantities (*e.g.*, turbulence kinetic energy), which are positive because of the underlying physics. The equations consist of convective, diffusive, and source term operators.

Despite their relatively simple mathematical representation, two-equation turbulence models present serious numerical difficulties, including convergence and positivity-preservation difficulties. The common argument is that the convergence difficulties arise mainly due to the strongly nonlinear source term, having time scales that greatly differ from those of the convective and diffusive terms. Furthermore, in the process of convergence, non-physical solutions, namely negative values of the turbulence quantities, may appear even if the analytical solution exists and is analytically guaranteed to remain positive [3]. These difficulties dramatically deteriorate convergence rates of the overall flow solver, requiring several thousands of iterations to reach the desired convergence criterion.

Therefore, one of the main challenges in modern computational fluid dynamics (CFD) lies in accelerating numerical methods for solving the mean-flow and turbulence model equations in cases where conventional methods are not optimal. One of the fastest acceleration means known today is use of multigrid methods (MG). MG methods accelerate convergence rates of numerical schemes by using a hierarchy of grids, based on the notion that certain numerical error modes are more efficiently treated on a coarse grid than on a fine grid. However, a coarse grid may only be used in conjunction with a finer one, requiring proper data transfer between successive grids.

MG methods rely on two basic principles: *Smoothing* and *Coarse Grid Correction (CGC)*. First, standard iterative methods (*e.g.*, Gauss-Seidel) with good smoothing (that is, elimination of high spatial frequency modes) properties are used to treat non-smooth errors in the solution. Pre-smoothing is required because only a smooth error is well represented both on fine and coarse grids, while non-smooth errors exhibit aliasing on coarse grids, significantly reducing the efficiency of CGC [4]. After a smooth error is obtained on the finest grid where a solution is sought, relaxation continues on coarser grids which are achieved by eliminating every other grid line in each coordinate direction. A coarse grid relaxation is substantially (up to four times in 2D) cheaper than its fine grid counterpart, and is also more efficient in eliminating errors which are relatively smooth on a finer grid. Thus, efficiency can be increased by transferring (*restricting*) some of the fine grid iterations required for convergence, to a coarser grid, and interpolating (*prolongating*) the results, that is, applying a coarse grid correction, to advance the solution on the finest grid.

While MG methods are well defined in a mathematical sense [5, 6], their efficient application for RANS equations with two-equation turbulence models is rather difficult. Among the barriers currently standing in the way of demonstrating an optimally efficient MG method for the RANS equations is the successful incorporation of turbulence transport equations in the multigrid framework [7].

There are two basic approaches to the incorporation of turbulence models in MG methods:

- Mean-flow multigrid (MF-MG)
- Fully-coupled multigrid (FC-MG)

In MF-MG [8, 9, 10], the mean-flow equations are solved on all grid levels, while the turbulence model equations are integrated only on the finest grid where a solution is sought, as in single-grid computations. In this approach, turbulence variables are simply injected onto coarser grids, where they are frozen. This allows bypassing numerical difficulties arising from the destabilizing effects of productive turbulence model source terms [11]. However, mean-flow equations convergence was proven to be highly influenced by turbulence model equations convergence [12]. Therefore, insufficient acceleration of the turbulence transport equations due to a partial use of single-grid computations in MF-MG may result in an overall reduced convergence rate, compared to fully-coupled multigrid.

An alternative to MF-MG, is the fully-coupled multigrid approach (FC-MG), in which both the mean-flow equations and the turbulence model equations are solved on all grid levels that are created in a multigrid framework. Although FC-MG is regarded as being more efficient in terms of convergence, its actual implementation is far from being straightforward. Usually, artificial stabilization techniques are used [13, 14, 15, 16] to overcome numerical difficulties encountered in integration of turbulence transport equations on coarse grid levels of the MG hierarchy. While these techniques increase stability of multigrid for the RANS equations coupled with two-equation turbulence models, they may also hinder convergence rates.

The present study focuses on designing a multigrid method for an implicit solver of the compressible RANS equations, together with a two-equation turbulence model. The work was guided by the belief that designing a robust multigrid method for this problem strongly depends on use of a highly stable scheme for the turbulence model equations. It was realized that some of the difficulties encountered in the multigrid solution of RANS turbulence models occur in fact due to the use of insufficiently stable relaxation schemes, rather than to the multigrid concept itself. Therefore, the unconditionally positive-convergent (UPC) time integration implicit scheme for turbulence transport equations developed by Mor-Yossef and Levy [17] is adopted in this work and successfully extended for use in multigrid methods, allowing for smooth incorporation of these equations in a multigrid framework for the RANS equations. The proposed method is based

on a Full Approximation Storage (FAS) fully-coupled multigrid approach (FC-MG). The method is nearly free of stabilization fixes and other techniques commonly used to avoid numerical difficulties.

2 GOVERNING EQUATIONS

The governing equations are obtained by Favre-averaging the Navier-Stokes equations (RANS) and modeling the Reynolds stress. The unknown Favre-averaging Reynolds stress tensor is modeled in this work via linear or non-linear two-equation turbulence models. The linear model used is the k-ω turbulence model developed by Kok [18], which is considered to be topology-free and was designed to resolve the well-known dependency on free-stream values of ω. The non-linear model used is based on Kok's model together with the Explicit Algebraic Reynolds Stress Model (EARSM) developed by Wallin and Johansson [19]. Hereafter the linear and non-linear turbulence models are referred to as $k\omega$-*Linear* and $k\omega$-$EARSM$, respectively.

In a compact conservation law form, the 2D RANS equations may be expressed in Cartesian coordinates as follows:

$$\frac{\partial \boldsymbol{\mathcal{Q}}}{\partial t} + \frac{\partial(\boldsymbol{\mathcal{F}}_c - \boldsymbol{\mathcal{F}}_d)}{\partial x} + \frac{\partial(\boldsymbol{\mathcal{G}}_c - \boldsymbol{\mathcal{G}}_d)}{\partial y} = \boldsymbol{\mathcal{S}} \tag{1}$$

The vector $\boldsymbol{\mathcal{Q}} = \{\mathbf{Q}, \mathbf{q}\}$ denotes the dependent variables vector of mean-flow equations, $\mathbf{Q}$, and of the turbulence model equations, $\mathbf{q}$, given as:

$$\mathbf{Q} = \begin{bmatrix} \rho \\ \rho u \\ \rho v \\ E \end{bmatrix} \quad , \quad \mathbf{q} = \begin{bmatrix} \rho k \\ \rho \omega \end{bmatrix} \tag{2}$$

The fluid density is denoted by ρ, the Cartesian velocity vector components are denoted by u and v, and E denotes the total energy. The turbulence kinetic energy is denoted by k. The second turbulence quantity is denoted by ω, representing the specific turbulence dissipation rate. The convective flux vectors are denoted by $\boldsymbol{\mathcal{F}}_c = \{\mathbf{F}_c, \mathbf{f}_c\}$ and $\boldsymbol{\mathcal{G}}_c = \{\mathbf{G}_c, \mathbf{g}_c\}$, where $\mathbf{F}_c$, $\mathbf{G}_c$ and $\mathbf{f}_c$, $\mathbf{g}_c$ are the mean-flow and turbulence model equations convective flux vectors, respectively:

$$\mathbf{F}_c = \begin{bmatrix} \rho u \\ \rho u u + p \\ \rho u v \\ u\,(E+p) \end{bmatrix} \quad , \quad \mathbf{G}_c = \begin{bmatrix} \rho v \\ \rho u v \\ \rho v^2 + p \\ v\,(E+p) \end{bmatrix} \tag{3}$$

$$\mathbf{f}_c = \begin{bmatrix} \rho u k \\ \rho u \omega \end{bmatrix} \quad , \quad \mathbf{g}_c = \begin{bmatrix} \rho v k \\ \rho v \omega \end{bmatrix} \tag{4}$$

The diffusive flux vectors are denoted as $\boldsymbol{\mathcal{F}}_d = \{\mathbf{F}_d, \mathbf{f}_d\}$ and $\boldsymbol{\mathcal{G}}_d = \{\mathbf{G}_d, \mathbf{g}_d\}$ where $\mathbf{F}_d$, $\mathbf{G}_d$ and $\mathbf{f}_d$, $\mathbf{g}_d$ are the mean-flow and turbulence model equations diffusive flux vectors, respectively:

$$\mathbf{F}_d = \begin{bmatrix} 0 \\ \tau_{xx} \\ \tau_{xy} \\ u\tau_{xx} + v\tau_{xy} + \kappa_d \frac{\partial T}{\partial x} \end{bmatrix} \quad , \quad \mathbf{G}_d = \begin{bmatrix} 0 \\ \tau_{xy} \\ \tau_{yy} \\ u\tau_{xy} + v\tau_{yy} + \kappa_d \frac{\partial T}{\partial y} \end{bmatrix} \tag{5}$$

$$\mathbf{f}_d = \begin{bmatrix} \mu_k \frac{\partial k}{\partial x} \\ \mu_\omega \frac{\partial \omega}{\partial x} \end{bmatrix} \quad , \quad \mathbf{g}_d = \begin{bmatrix} \mu_k \frac{\partial k}{\partial y} \\ \mu_\omega \frac{\partial \omega}{\partial y} \end{bmatrix} \tag{6}$$

The fluid temperature is denoted by T and $\kappa_d = \kappa_l + \kappa_t$ represents the thermal conductivity of the fluid with κ_l and κ_t being the molecular and turbulent thermal conductivity coefficients, respectively. The shear stresses are defined as:

$$\tau_{xx} = 2\left(\mu + \mu_t\right)\frac{\partial u}{\partial x} - \frac{2}{3}\left(\mu + \mu_t\right)\left(\frac{\partial u}{\partial x} + \frac{\partial v}{\partial y}\right) - \frac{2}{3}\rho k + \psi\tau_{xx}^{nl} \tag{7}$$

$$\tau_{yy} = 2\left(\mu + \mu_t\right)\frac{\partial v}{\partial y} - \frac{2}{3}\left(\mu + \mu_t\right)\left(\frac{\partial u}{\partial x} + \frac{\partial v}{\partial y}\right) - \frac{2}{3}\rho k + \psi\tau_{yy}^{nl} \tag{8}$$

$$\tau_{xy} = \left(\mu + \mu_t\right)\left(\frac{\partial u}{\partial x} + \frac{\partial v}{\partial y}\right) + \psi\tau_{xy}^{nl} \tag{9}$$

where τ_{xx}^{nl}, τ_{xy}^{nl}, and τ_{yy}^{nl} represent the supplementary high order terms used in the EARSM model, and the scalar ψ distinguishes between the linear ($\psi = 0$) and non-linear ($\psi = 1$) models. The molecular viscosity, μ, is calculated from Sutherland's law, and μ_t denotes the turbulent viscosity. The turbulence diffusive flux vector coefficients μ_k, μ_ω are defined as:

$$\mu_k = \mu + \frac{\mu_t}{\sigma_k} \tag{10}$$

$$\mu_\omega = \mu + \frac{\mu_t}{\sigma_\omega} \tag{11}$$

where σ_k, σ_ω are model-specific closure coefficients. The mean-flow equations are closed using the equation of state for a perfect gas, given by:

$$p = \left[E - \frac{1}{2}\rho\left(u^2 + v^2\right)\right](\gamma - 1) \tag{12}$$

where γ is the ratio of specific heats (c_p/c_v), set to $\gamma = 1.4$. In the flows examined in this work, source terms appear only due to turbulence model equations. Therefore, the source-term vector $\boldsymbol{\mathcal{S}}$ is represented by:

$$\boldsymbol{\mathcal{S}} = \begin{bmatrix} 0 & 0 & 0 & 0 & S_k & S_\omega \end{bmatrix}^T \tag{13}$$

Detailed formulation of the source-term and model-specific constants may be found in the original publications [18, 19].

3 NUMERICAL METHOD

A conservative cell-centered finite volume methodology is employed to discretize the governing equations on structured grids. Let C_a denote the control area (defined by a grid area element), and let $\partial\Gamma$ denote the control area boundary, with $\mathbf{n} = [n_x, n_y]^T$ being the outward-pointing unit normal vector to $\partial\Gamma$. Therefore, the integral form of Eq. (1) for a control area C_a can be expressed as:

$$\frac{\partial}{\partial t}\int_{C_a} \boldsymbol{\mathcal{Q}}\ dA + \int_{\partial\Gamma} \left(\boldsymbol{\mathcal{H}}_c - \boldsymbol{\mathcal{H}}_d\right)\ dl = \int_{C_a} \boldsymbol{\mathcal{S}}\ dA \tag{14}$$

where $\boldsymbol{\mathcal{H}}_c = \boldsymbol{\mathcal{F}}_c n_x + \boldsymbol{\mathcal{G}}_c n_y$, and $\boldsymbol{\mathcal{H}}_d = \boldsymbol{\mathcal{F}}_d n_x + \boldsymbol{\mathcal{G}}_d n_y$.

3.1 Spatial Discretization

The semi-discrete form of Eq. (14) for cell i of a non-deforming grid is given by:

$$A_i \frac{d\,\boldsymbol{\mathcal{Q}}_i}{dt} = -\sum_{j\in N(i)} \left(\boldsymbol{\mathcal{H}}_{c_{ij}} - \boldsymbol{\mathcal{H}}_{d_{ij}}\right) l_{ij} + \boldsymbol{\mathcal{S}}_i A_i \equiv \boldsymbol{\mathcal{R}}_i \tag{15}$$

where $\boldsymbol{\mathcal{Q}}_i$ is the vector of cell-averaged conservative variables, and $\boldsymbol{\mathcal{S}}_i$ is the cell source vector. The terms $\boldsymbol{\mathcal{H}}_{c_{ij}}$ and $\boldsymbol{\mathcal{H}}_{d_{ij}}$ are the convective and diffusive fluxes, respectively, normal to the interface ij shared by cell i and its neighboring cell j. A_i is the cell area, and t represents the time. The term l_{ij} is the face length of the interface ij, and $N(i)$ denotes the set of cell i's neighbors (direct face neighbors). The vector $\boldsymbol{\mathcal{R}}_i$ signifies the right hand side (residual) of the equation set:

$$\boldsymbol{\mathcal{R}}_i = \left\{\mathbf{R}^T, \mathbf{r}^T\right\}_i^T \tag{16}$$

where $\mathbf{R}$ represents the residual of the mean-flow equations, and $\mathbf{r}$ represents the residual of the turbulence model equations.

The convective flux vector of the mean-flow equations is computed at the cell interface using the HLLC scheme proposed by Batten et al. [20]. The diffusive flux vector of the mean-flow equations is discretized by employing central differencing based on the diamond stencil [21]. The convective flux vector of the turbulence model equations is computed based on the first-order passive scalar approach [22], within the HLLC numerical framework [20]. The turbulence model diffusive flux vector is evaluated according to the thin-layer approximation.

3.2 Time Integration

Implicit time marching of both the mean-flow, and the turbulence model discretized equations is employed, based on the first order implicit backward Euler method:

$$\left[\frac{A}{\Delta t}\mathcal{I} - \frac{\partial \boldsymbol{\mathcal{R}}}{\partial \boldsymbol{\mathcal{Q}}}\right]^n \Delta\,\boldsymbol{\mathcal{Q}}^n = \boldsymbol{\mathcal{R}}^n \tag{17}$$

where $\mathcal{I}$ is the identity matrix, and the Δ operator is defined as the increment between time levels n and n+1. Equation (17) is solved using the alternating line symmetric Gauss-Seidel method, in a loosely coupled manner. Loosely coupled time integration possesses several advantages over a coupled strategy. It is easy to implement and it provides the enhanced flexibility required to design a stable and efficient scheme for the turbulence model equations.

3.2.1 Mean-Flow Equations Time Integration

The algebraic set of the discretized mean-flow equations may be written as:

$$\left[\frac{A}{\Delta t}\mathcal{I} - \frac{\partial \mathbf{R}}{\partial \mathbf{Q}}\right]^n \Delta \mathbf{Q}^n = \mathbf{R}^n \tag{18}$$

The evaluation of the exact Jacobian $\frac{\partial \mathbf{R}}{\partial \mathbf{Q}}$, of the high-order, nonlinear explicit operator $\mathbf{R}$ is very complicated. To alleviate this difficulty, the common practice is to approximate the Jacobian using the spatial lower-order accuracy of the explicit operator, meaning that the approximated Jacobian of the convective part is based on a first-order spatial accuracy of the convective explicit operator. The Jacobian of the diffusive part is based on the thin-layer approximation, namely, the approximated Jacobian is based on a compact stencil which takes into account only direct face neighbors. Moreover, the non-linear Reynolds-stress tensor that appears in the mean-flow equations is treated implicitly only with regard to its linear part. The remaining high-order terms, namely τ_{xx}^{nl}, τ_{xy}^{nl} and τ_{yy}^{nl}, are treated explicitly. In the current work, the approximated Jacobian of the mean-flow convective part is evaluated using the HLLC Jacobian by Batten et al. [20]. The diffusive part of the Jacobian is calculated analytically. An implicit treatment of boundary conditions is employed only for wall boundaries. To improve iterative convergence to a steady state solution, the B2 scheme proposed by Batten et al. [20] is used.

3.2.2 Turbulence Model Equations Time Integration Method

Similarly to the algebraic set of the discretized mean-flow equations, the algebraic set of the discretized turbulence model equations is given by:

$$\left[\frac{A}{\Delta t}\mathcal{I} - \frac{\partial \mathbf{r}}{\partial \mathbf{q}}\right]^n \Delta \mathbf{q}^n = \mathbf{r}^n \tag{19}$$

A straightforward implementation of the turbulence model equations' exact Jacobian, $\frac{\partial \mathbf{r}}{\partial \mathbf{q}}$, usually leads to an unstable scheme that exhibits convergence and positivity preserving difficulties. These numerical difficulties are even further amplified in a multigrid framework. Any lagging in the turbulence model time integration, with respect to that of the mean-flow equations, may hinder the convergence rate. Therefore, a highly stable implicit

scheme for the turbulence model equations is vital for the success of FC-MG computations. It should be noted that the B2 scheme is not used for time integration of the turbulence model equations, and therefore Eq. (19) is employed only in the second step of the B2 scheme of the mean-flow equations.

In this work, the unconditionally positive-convergent (UPC) time integration implicit scheme for turbulence transport equations developed by Mor-Yossef and Levy [17] is adopted and successfully extended for use in multigrid methods. The key idea of the UPC scheme is the design of the implicit operator to form an M-matrix [23]. Specifically, the Jacobian, $-\frac{\partial \mathbf{r}}{\partial \mathbf{q}}$, is approximated by a matrix $\mathcal{M} \approx -\frac{\partial \mathbf{r}}{\partial \mathbf{q}}$ such that it fulfills the following two conditions:

1. $\mathcal{M}$ is an M-matrix
2. $\mathbf{r} + \mathcal{M}\mathbf{q}$ is a non-negative vector (*i.e.*, all its entries are non-negative)

By substituting the matrix $\mathcal{M}$ for the matrix $-\frac{\partial \mathbf{r}}{\partial \mathbf{q}}$, Eq. (19) may be rewritten as:

$$\left[\frac{A}{\Delta t}\mathcal{I} + \mathcal{M}\right]^n \Delta \mathbf{q}^n = \mathbf{r}^n \tag{20}$$

Eq. (20) represents an unconditionally positive-convergent scheme. Complete details of the proof and construction may be found in Ref. [24].

4 MULTIGRID METHOD

For nonlinear equations such as the RANS and turbulence model equation set, the Full Approximation Storage (FAS) multigrid algorithm [25] is mostly used. In multigrid methods, a hierarchy of grids is constructed based on successive coarsening (*e.g.*, elimination of every other grid line, in each direction) of a given fine grid of mesh size h. The resulting grids are of typical mesh sizes $2h, 4h, 8h, etc.$ Normally, 4 fine-grid cells compose a single underlying coarse-grid cell.

The numerical solution is sought on the finest grid in the hierarchy, while the underlying coarse meshes are used to damp low-frequency error modes that can not be efficiently reduced using fine-grid relaxations. Pseudo-time iterations (*i.e.*, Gauss-Seidel relaxation, as described in sections 3.2.1, 3.2.2) are employed on all grid levels to smooth errors of wavelengths comparable to the corresponding mesh size. As a result, the entire error spectrum is reduced at a comparable rate, leading to notably faster convergence characteristics.

The governing equations, given in integral form in Eq. (14), may be rewritten in operator notation as:

$$\frac{\partial}{\partial t}\int_{C_a} \boldsymbol{\mathcal{Q}}\ dA = \underbrace{-\left[\int_{\partial\Gamma} (\boldsymbol{\mathcal{H}}_c - \boldsymbol{\mathcal{H}}_d)\ dl - \int_{C_a} \boldsymbol{\mathcal{S}}\ dA\right]}_{\boldsymbol{\mathcal{N}}(\boldsymbol{\mathcal{Q}})} \tag{21}$$

Where $\boldsymbol{\mathcal{N}}\left(\boldsymbol{\mathcal{Q}}\right)$ is a nonlinear operator representing the RANS and turbulence model equations, operating on the dependent-variable vector $\boldsymbol{\mathcal{Q}}$. The equivalent discrete operator, sampled on a grid of mesh size h, is denoted by $\boldsymbol{\mathcal{N}^h}\left(\boldsymbol{\mathcal{Q}^h}\right)$.

4.1 Basic Multigrid Algorithm

The basic multigrid algorithm employed in this work is based on a *V-Cycle* composed of pre-relaxation, restriction, coarse-grid correction and post-relaxation. Each V-cycle is based on recursively invoking the following two-grid algorithms where h and H denote fine and coarse grid levels, respectively.

Fine-grid pre-relaxation: $\boldsymbol{\mathcal{N}^h}\left(\boldsymbol{\bar{\mathcal{Q}}^h}\right) = -\boldsymbol{\mathcal{R}^h}$

Pre-relaxation sweeps are performed on the fine-grid to achieve an approximate solution $\boldsymbol{\bar{\mathcal{Q}}^h}$ and a corresponding smooth numerical residual $\boldsymbol{\mathcal{R}^h}$. One or two pre-relaxation sweeps are necessary to ensure that transferred fine-grid defects (residuals) are correctly sampled on coarser grids in the hierarchy, with relatively small aliasing.

Restriction to a coarser grid: $\boldsymbol{\mathcal{N}^H}\left(\boldsymbol{\mathcal{I}_h^H}\boldsymbol{\mathcal{Q}^h}\right) - \boldsymbol{\mathcal{N}^H}\left(\boldsymbol{\mathcal{I}_h^H}\boldsymbol{\bar{\mathcal{Q}}^h}\right) = \boldsymbol{\widetilde{\mathcal{I}}_h^H}\left(\boldsymbol{\mathcal{R}^h}\right)$

Using numerical restriction operators, appropriate coarse-grid equations are constructed to reduce low-frequency fine-grid errors. An area-weighted restriction operator $\boldsymbol{\mathcal{I}_h^H}$ is employed to transfer the current fine-grid approximate solution $\boldsymbol{\bar{\mathcal{Q}}^h}$ to a coarser grid. The transferred fine grid residual, $\widetilde{\mathcal{I}}_h^H\left(\mathcal{R}^h\right)$, is calculated by summing four equivalent fine-grid residuals.

Coarse-grid relaxations: $\boldsymbol{\mathcal{N}^H}\left(\boldsymbol{\bar{\mathcal{Q}}^H}\right) = \underbrace{\boldsymbol{\mathcal{N}^H}\left(\boldsymbol{\mathcal{I}_h^H}\boldsymbol{\bar{\mathcal{Q}}^h}\right) + \boldsymbol{\widetilde{\mathcal{I}}_h^H}\left(\boldsymbol{\mathcal{R}^h}\right)}_{\boldsymbol{Fine-grid\ Constants}} - \boldsymbol{\mathcal{R}^H}$

The coarse-grid equation is solved using local iterations, starting from the initial solution $\boldsymbol{\bar{\mathcal{Q}}_0^H} = \boldsymbol{\mathcal{I}_h^H}\boldsymbol{\bar{\mathcal{Q}}^h}$. Coarse-grid relaxations yield an approximate solution $\boldsymbol{\bar{\mathcal{Q}}^H}$, and a corresponding coarse-grid residual $\boldsymbol{\mathcal{R}^H}$. Note that the first iteration on the coarse-grid is driven only by $\boldsymbol{\widetilde{\mathcal{I}}_h^H}\left(\boldsymbol{\mathcal{R}^h}\right)$, since $\boldsymbol{\mathcal{N}^H}\left(\boldsymbol{\bar{\mathcal{Q}}_0^H}\right) = \boldsymbol{\mathcal{N}^H}\left(\boldsymbol{\widetilde{\mathcal{I}}_h^H}\boldsymbol{\bar{\mathcal{Q}}^h}\right)$. Note that the first two expressions on the right-hand-side of the coarse-grid equation, which originate from the fine-grid, remain constant throughout coarse-grid relaxations.

Numerical tests showed that for this problem, FAS multigrid does not require a direct and most accurate solution on the coarsest grid to ensure efficient acceleration. In fact, attempts to use a large number of iterations in order to achieve an accurate solution on the coarsest grid yield unrealistically large values of turbulent viscosity originating from large initial fine-grid turbulence defects contributing to uncontrolled turbulence production on coarser grids.

Coarse-grid correction: $\boldsymbol{\Delta\bar{\mathcal{Q}}^h = \mathcal{I}_H^h\left(\bar{\mathcal{Q}}^H - \mathcal{I}_h^H\bar{\mathcal{Q}}^h\right)}$

The approximate coarse-grid solution $\bar{\mathcal{Q}}^H$ is transfered (*prolongated*) back to the fine-grid, where it is used to correct the current fine-grid solution $\bar{\mathcal{Q}}^h$. The prolongation operator is based on bi-linear interpolation. One should bear in mind that for the commonly used two-equation turbulence models (such as the k-ω and the k-ϵ) the turbulence model quantities vary strongly near the wall. Therefore, bi-linear interpolation may not be sufficiently accurate. Modified interpolations may alleviate this issue by offering better representation of large near-wall gradients.

Fine-grid post-relaxation: $\boldsymbol{\mathcal{N}^h\left(\bar{\mathcal{Q}}^h\right) = -\mathcal{R}^h}$

Aside from valuable corrections, application of a coarse-grid correction also introduces new errors to the fine-grid solution, arising from interpolation inaccuracies. Several post-iterations are performed to reduce these new errors. In the present work it was found that at least four post-relaxations are required to efficiently reduce the new error components introduced by interpolating and applying a coarse-grid correction.

4.2 Extension of the UPC Scheme for Multigrid

The original UPC scheme ensures positivity and convergence for time-integration of turbulence model equations in single-grid computations. However, in multigrid, a modification of the UPC scheme is required to retain the positivity of turbulence variables on coarse grid levels as well. On coarse grid levels, forcing terms (transferred fine-grid residuals, and residuals calculated based on the transferred solution) of the turbulence model equations may be regarded as additional source terms. Unless they are appropriately treated they may cause loss of positivity of turbulence variables. Hereafter, an appropriate numerical treatment of these terms is presented, aimed at extending the UPC scheme for use in multigrid methods.

Let $\boldsymbol{n(q)}$ denote the non-linear discrete operator representing the turbulence model equations alone, correspondingly operating on the turbulence variables vector $\boldsymbol{q}$ (similar to equation (21)). A typical discrete coarse-grid equation for the turbulence variables is of the form:

$$\boldsymbol{n^H\left(\bar{q}^H\right) = \underbrace{n^H\left(\mathcal{I}_h^H\bar{q}^h\right) + \widetilde{I}_h^H\left(r^h\right)}_{forcing\ term} - r^H} \tag{22}$$

Where the forcing term (labeled in equation (22)) denoted by,

$$\boldsymbol{c^H \equiv [c_k, c_w] \triangleq n^H\left(\mathcal{I}_h^H\bar{q}^h\right) + \widetilde{I}_h^H\left(r^h\right)} \tag{23}$$

is a constant vector. Consequently, the time-marching delta-form of the discretized turbulence model equations on the coarse grid level is given in (the index H is hereafter

omitted for convenience):

$$\left[\frac{A}{\Delta t}\mathcal{I}+\mathcal{M}\right]^n \Delta\mathbf{q}^n = \mathbf{r}^n - \mathbf{c} \tag{24}$$

The motivation is to modify the implicit operator to appropriately account for the *new* source term, in the form of vector $\mathbf{c}$. First, the vector $(-\mathbf{c})$ is decomposed to positive and negative parts as follows:

$$-\mathbf{c} = \mathbf{c}_P - \mathbf{c}_N \tag{25}$$

where $\mathbf{c}_P$ and $\mathbf{c}_N$ are defined as:

$$\mathbf{c}_P = \frac{1}{2}\left[|-\mathbf{c}| + (-\mathbf{c})\right] \tag{26}$$

$$\mathbf{c}_N = \frac{1}{2}\left[|-\mathbf{c}| - (-\mathbf{c})\right] \tag{27}$$

The resulting set of equations is:

$$\left[\frac{A}{\Delta t}\mathcal{I}+\mathcal{M}\right]^n \Delta\mathbf{q}^n = \mathbf{r}^n + \mathbf{c}_P - \mathbf{c}_N \tag{28}$$

For the purpose of extending the UPC scheme for use on coarse-grid levels, the implicit delta form of equation (28) is split and rewritten as follows (assuming $\Delta t \to \infty$):

$$\mathcal{M}^n\mathbf{q}^{n+1} = \mathbf{r}^n + \mathcal{M}^n\mathbf{q}^n + \mathbf{c}_P - \mathbf{c}_N \tag{29}$$

The stabilizing term originating from discretization of the time derivative is dropped in order to ensure an unconditionally positive-convergent scheme. Bearing in mind that the basic UPC scheme (designed for single-grid computations) ensures that the vector $\mathbf{r}^n + \mathcal{M}^n\mathbf{q}^n$ is non-negative, on coarse-grid levels, the presence of the additional constant vector $-\mathbf{c}_N$ may not meet the condition of a non-negative right-hand side of the non-delta form equation, namely that the right hand side vector of Eq. (29) will be non-negative. By approximating $\mathbf{c}_N$ as:

$$\mathbf{c}_N \approx \mathcal{C}\mathbf{q}^{n+1} \tag{30}$$

where the matrix $\mathcal{C}$ is defined as follows:

$$\mathcal{C} = \begin{bmatrix} \frac{(c_k)_N}{(\rho k)^n} & 0 \\ 0 & \frac{(c_\omega)_N}{(\rho\omega)^n} \end{bmatrix} \tag{31}$$

equation (29) may be recast as

$$\left[\mathcal{M}+\mathcal{C}\right]^n \mathbf{q}^{n+1} = \mathbf{r}^n + \mathcal{M}^n\mathbf{q}^n + \mathbf{c}_P \tag{32}$$

Since the left-hand side matrix, $[\mathcal{M}+\mathcal{C}]$ is also an M-matrix, and since the right-hand side vector of Eq. (32), $\mathbf{r}^n + \mathcal{M}^n\mathbf{q}^n + \mathbf{c}_P$, is non-negative, positivity of the vector $\mathbf{q}^{n+1}$

is unconditionally guaranteed. Finally, the delta form of the extended UPC scheme for coarse-grid levels is attained by adding the vector -$\mathcal{C}^n\mathbf{q}^n(\equiv -\mathbf{c}_N)$ to both sides of equation (32), and returning the vector $\mathcal{M}^n\mathbf{q}^n$ to its original place on the left-hand side of the equation:

$$\left[\frac{A}{\Delta t}\mathcal{I} + \mathcal{M} + \mathcal{C}\right]^n \Delta\mathbf{q}^n = \mathbf{r}^n - \mathbf{c} \tag{33}$$

Although, Eq. (33) guarantees positivity and convergence for any time step, in practice it was found that using an infinite time step for the turbulence model equations results in an excessive and unrealistic build-up of turbulent viscosity values on coarse-grid levels. This anomaly was mainly noted during early stages of the simulation when the transferred fine-grid defects are still large. However, numerical experiments show that stable simulations can be achieved with a turbulence model CFLT number as high as twice the CFL number that is used for the mean-flow equations. It should be emphasized that realizability constraints [26] that were derived for the basic turbulence model are not adequate for coarse-grid levels, since the additional fine grid defect may be regarded as an additional source or production term, which the basic realizability constraints do not account for. This is believed to be the origin of the excessive build-up of turbulent viscosity on coarse grid levels.

5 NUMERICAL EXAMPLES

Two well-known test cases are simulated and examined using the proposed multigrid method. The aim of the tests is twofold: first to study the convergence characteristics of the new multigrid algorithm; and second, to verify that the proposed procedure indeed preserves the positivity of the turbulence variables. The first test case is the separated flow about the NACA4412 airfoil at high incidence. The second test is the transonic flow about the RAE2822 airfoil. Several general remarks and definitions should be made prior to proceeding:

- The *convergence* criterion was set to a drop of eight orders in the magnitude of the mean-flow equations residual, compared to the initial residual.
- Convergence was measured in normalized *work units (WU)*, each equal to the computational time that is required to perform a single fine-grid relaxation sweep.
- A uniform CFL number was used on all grid levels of a given simulation. The maximum CFL (as stated in the description of the simulation) was achieved after 10 cycles, or 40 iterations, in multigrid and single-grid simulations, respectively.
- A multigrid hierarchy of 3 grid levels was used in all simulations that were conducted in this work. In addition, a hierarchy of 4 grid levels was used in two of the test-cases (marked by "MG 4L").

- It is important to emphasize that in all conducted simulations, no clipping of turbulence variables was employed, nor were there any bounds enforced on turbulence model terms.

5.1 Boundary and Initial Conditions

Characteristic boundary conditions based on the Riemann invariant are used for the mean-flow equations, and enforced at subsonic inflow and outflow regions. The inflow turbulence kinetic energy is evaluated according to the relation $k = \frac{3}{2}(Tu \cdot U_\infty)^2$ where Tu represents the turbulence intensity. The inflow turbulence dissipation rate is set so that normalized inflow turbulent viscosity is equal to $\mu_{t\,\infty} = 0.01$. At the outflow boundary, turbulence variables are extrapolated from interior values. Wall boundary conditions for the turbulence kinetic energy are set to $k = 0$, while the turbulence dissipation rate at the wall is determined following the treatment proposed in Ref. [27]:

$$\omega_{wall} = CN\frac{19}{9}\frac{6\nu_{wall}}{\beta\left(\Delta y_1\right)^2} \tag{34}$$

where $CN = 0.1 \times min\left[50, max(10, Re_\infty \Delta y_1 - 20)\right]$, $Re_\infty \Delta y_1$ is the cell Reynolds number and Δy_1 denotes the distance to the first cell center neighboring the wall, as measured from the wall. The initial solution of the mean-flow equations and of the turbulence model equations is set to uniform free-stream flow throughout the flow-field.

5.2 NACA4412 airfoil

Simulation of the flow about a NACA4412 airfoil at high incidence is a well-known test for a solver's ability to accurately resolve high lift separated flows. In the current work, flow about the airfoil at an incidence of $\alpha = 13.87°$, a Mach number of $M_\infty = 0.2$ and a Reynolds number of $Re_\infty = 1.52 \times 10^6$ is simulated using the $k\omega$-*Linear* turbulence model, and compared to the experimental results of Ref. [28]. Two different grid topologies were examined: a C-type grid, and an O-type grid. Common grid parameters are given in Table 1. At experimental flow conditions [28], a steady trailing-edge separation is present.

Grid name	Grid dim.	Far-field	Δy_1	y^+
C-type grid	243×67	14 chords	5×10^{-6}	≤ 1
O-type grid	283×95	25 chords	3×10^{-6}	≤ 0.62

Table 1: NACA4412 computational grid information

Figure 1 shows a comparison of calculated stream-wise velocity profiles and experimental data at four stations along the upper airfoil surface (η represents the axis perpendicular to the airfoil surface). The numerical results appear to be in good agreement with the experimental results. Specifically, the velocity profile at the separation region is accurately predicted.

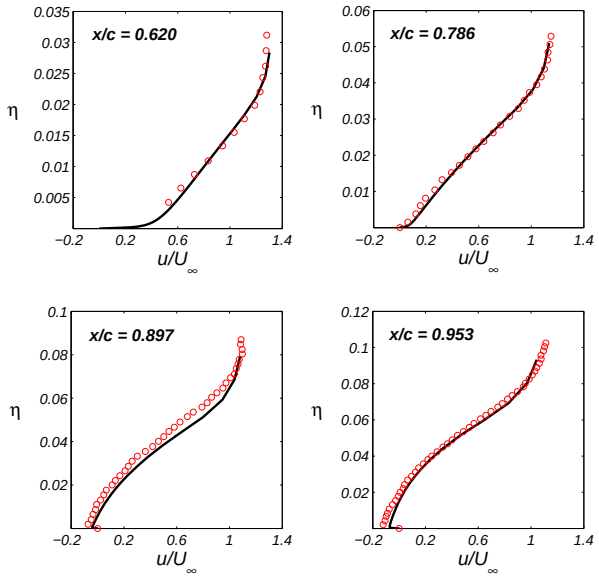

Figure 1: Comparison between calculated and measured stream-wise velocity profiles at four stations along the upper NACA4412 airfoil surface: ∘, experiment [28], — computation.

A comparison of convergence histories recorded using the single-grid and multigrid methods is given in Figure 2, for both the C-type and O-type grids. Note that a 4 level MG hierarchy was also evaluated using the O-type grid. The simulations were conducted with a mean-flow CFL as high as CFL=400. While the CFL of the turbulence model (CFLT) was as high as CFLT=800 in multigrid computations, and CFLT $\to \infty$ in single-grid computations. An acceleration factor of two was obtained for tests performed with the C-grid. Moreover, while the SG solver failed to reach convergence using the O-type grid (even with lower CFL and CFLT numbers), the 3 level MG solver converged using the same grid in only 343 work units, corresponding to 53 MG cycles. The 4 level MG solver converged in 312 work units, corresponding to 44 MG cycles. Hence, in this case, further acceleration of 10% is achieved through use of a 4 level MG hierarchy, compared to use of a 3 level MG hierarchy. The similarity of MG performance for both topologies (C-type and O-type grids) indicates the robustness and consistency of the proposed method. Noteworthy is the fact that the convergence characteristics of the mean-flow equations and of the turbulence model equations are similar. Consequently, it is recognized that stability and convergence of the mean-flow equations and of the turbulence model equations are in some sense coupled. This can be realized from the fact that, although these two sets of equations are solved in a loosely-coupled time marching manner, their multigrid cycling is strongly coupled. Furthermore, it is well known that due to the high numerical stiffness of turbulence model equations, turbulent simulations converge slowly as they require the use of smaller time steps along with the need to closely follow the evolution of the simulation. In contrast, the use of the UPC scheme completely overturns the trend. The ability to utilize a very large time step for the turbulence model solver guarantees fast convergence

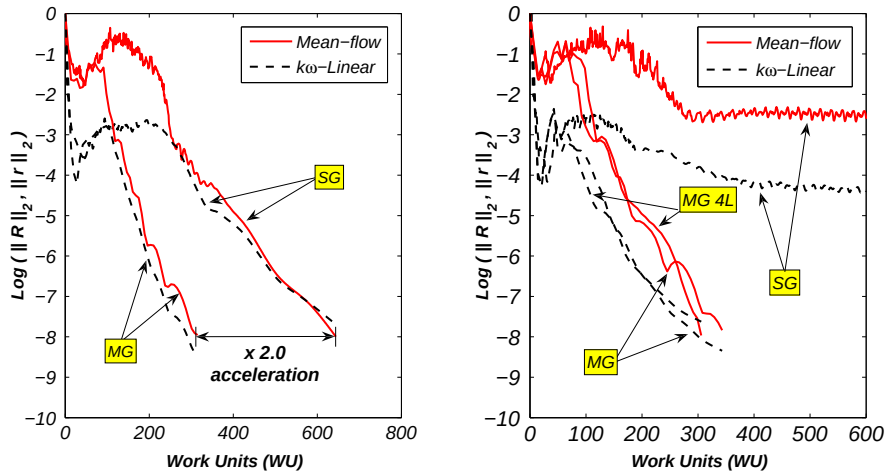

(a) C-Grid (b) O-Grid

Figure 2: Comparison of convergence histories for the NACA4412 airfoil at $Re_\infty = 1.52\times10^6$, $M_\infty = 0.2$, $\alpha = 13.87^o$, MG(CFL=400,CFLT=800) vs. SG(CFL=400,CFLT=∞).

of the turbulence equations, with respect to the current mean flow state. This is achieved while guaranteeing positivity of turbulence quantities. Thus, apart from stabilizing time-integration of turbulence model equations, use of the UPC scheme also brings about an accelerated convergence of the mean-flow equations as well.

5.3 RAE2822 airfoil

The simulation of the transonic flow about the RAE2822 supercritical airfoil is another well-known test case. The experiment performed by Cook *et al.* [29] covers a wide variety of flow conditions. In this work, flow at Mach number, $M_\infty = 0.734$, Reynolds number, $Re_\infty = 6.5\times10^6$, and an incidence angle of $\alpha = 2.54°$ (referred to as case 9 in Ref. [29]) was simulated using the proposed method, with the $k\omega$-*Linear* and $k\omega$-$EARSM$ turbulence models. Two C-type grids were employed in the current test: a fine grid, and a coarser grid. Common grid parameters are given in Table 2.

Grid name	Grid dim.	Far-field	Δy_1	y^+
Coarse grid (C)	275 × 67	31 chords	5×10^{-6}	≤ 1.9
Fine grid (C)	435 × 123	23 chords	1×10^{-6}	≤ 0.43

Table 2: RAE2822 computational grid information

A comparison of the calculated surface pressure coefficient with the experimental data [29] is displayed in figure 3. The overall agreement between computational and experimental data is very good. Specifically, the shock wave location is accurately captured. A comparison of convergence histories recorded using the single-grid and multigrid methods, with the $k\omega$-*Linear* turbulence model, is presented in Figure 4. The simulations were conducted with a maximum mean-flow CFL=200. the CFL of the turbulence

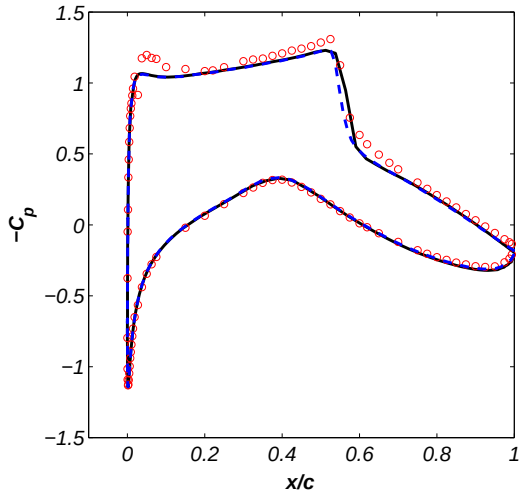

Figure 3: Comparison between C_p distributions on the RAE2822 airfoil; ∘, experiment (Cook, 1979); - - -, computation with $k\omega$-$EARSM$ turbulence model (fine-grid); —, computation with $k\omega$-$Linear$ turbulence model (fine-grid)

model (CFLT) was as high as CFLT=400 in multigrid computations, and CFLT $\rightarrow \infty$ in single-grid computations. Acceleration factors of nearly three times are obtained using the coarse and fine grids. Note that a 4 level MG hierarchy was also evaluated using the fine grid.

Strong evidence as to the robustness of the proposed MG algorithm can also be seen by noting that 3 level MG converges on the two examined grids in 245 and 357 work units (corresponding to 38 and 51 cycles) for the coarse and fine grid, respectively. On the other hand, single grid simulations yielded slower convergence using the fine grid than that achieved with the coarse grid, as expected. The 4 level MG solver converged in 291 work units on the fine grid, corresponding to 41 MG cycles. Hence, in this case, further acceleration of 18% is achieved through use of a 4 level MG hierarchy, compared to use of a 3 level MG hierarchy. In addition, it can be seen that SG computations on the fine grid suffer from noticeable convergence oscillations, while MG convergence remains smooth.

A comparison of convergence histories obtained using the SG and MG methods, with the $k\omega$-$EARSM$ turbulence model, on the coarse RAE2822 grid is presented in Figure 5. While a maximum CFL=200 and CFLT=400 were allowed in multigrid computations, only CFL=50 and CFLT=100 were allowed in single-grid computations. Acceleration factors of nearly two are achieved using the MG method, with respect to an equivalent SG simulation. The robustness of the proposed FC-MG-UPC method is once again shown in the fact that its suitable for both the non-linear (EARSM) turbulence model, as well as for the linear turbulence model, without requiring unique numerical treatment or stabilization fixes for any of the models. In addition, it should be noted that use of the proposed method also provides similar acceleration factors for both turbulence models examined in

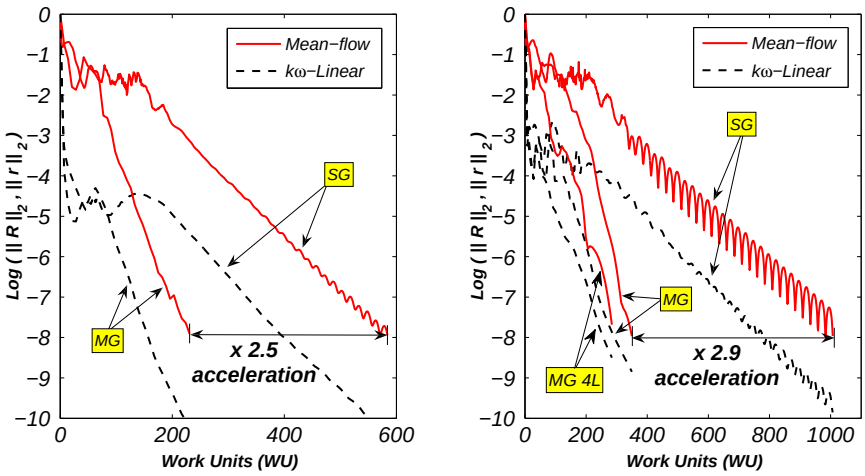

(a) Coarse Grid (b) Fine Grid

Figure 4: Comparison of convergence histories obtained using the $k\omega$-*Linear* turbulence model for the RAE2822 airfoil at $M_\infty = 0.734$, $Re_\infty = 6.5 \times 10^6$, and $\alpha = 2.54°$ (referred to as case 9 in Ref. [29]), MG(CFL=200,CFLT=400) vs. SG(CFL=200,CFLT=∞).

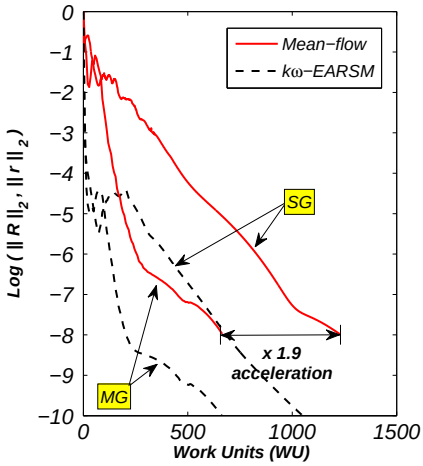

Figure 5: Comparison of convergence histories obtained using the $k\omega$-*EARSM* turbulence model for the RAE2822 airfoil at $M_\infty = 0.734$, $Re_\infty = 6.5 \times 10^6$, and $\alpha = 2.54°$ (referred to as case 9 in Ref. [29]), MG(CFL=200,CFLT=400) vs. SG(CFL=50,CFLT=100).

this work, with respect to an equivalent SG method.

6 Summary

A robust multigrid method for the solution of RANS equations with two equation turbulence models is presented. The method employs a basic relaxation scheme (alternating line Gauss-Siedel) where mean-flow and turbulence model equations are marched in time in a loosely-coupled manner. Two pillars stand at the base of the proposed MG method: Use of an extended version of the unconditionally positive-convergent scheme for two-equation turbulence models, adapted for use in multigrid, and the use of a strongly coupled multigrid cycling strategy. Minimal stabilization in the form of damping of turbulence equations coarse grid corrections was found to be necessary in order to ensure the positivity of turbulence quantities. The resulting MG method, termed FC-MG-UPC, is suitable for robust simulations of a wide range of flows thanks to being nearly free of artificial stabilization techniques, and user-supplied parameters. Numerical experiments showed that the proposed FC-MG-UPC method increases the efficiency compared to an equivalent single-grid method based on the UPC scheme by a factor of up to three. Moreover, the method has proven to be more stable than an equivalent SG-based method, allowing the use of higher CFL numbers for the mean-flow equations and even rapid convergence in a case where the SG-based method failed to converge. Thanks to the added stability gained by the use of the UPC scheme, a uniform CFL number and second order spatial accuracy could be used on all grid levels of the MG hierarchy. Moreover, the robustness of the proposed FC-MG-UPC method is well reflected by its impressive performance with the non-linear, $EARSM$, turbulence model, which is considered to be more numerically stiff than linear models.

7 ACKNOWLEDGMENTS

The authors would like to thank Dr. Yuval Levy for his valuable comments.

REFERENCES

[1] D. C. Wilcox, Turbulence modeling for CFD (Second edition), DCW Industries, Inc. 5354 Palm Drive, La Canada, California 91011, 1998.

[2] B. E. Launder, B. I. Sharma, Application of the energy-dissipation model of turbulence to the calculation of flow near a spinning disc, Letters in Heat and Mass Transfer 1 (1974) 131–138.

[3] Z.-N. Wu, S. Fu, Positivity of k-epsilon turbulence models for incompressible flow, Mathematical Models and Methods in Applied Sciences 12 (3) (2002) 393–406.

[4] I. Yavneh, Why multigrid methods are so efficient, Computing in Science & Engineering 8 (6) (2006) 12–22.

[5] W. Briggs, S. McCormick, A Multigrid Tutorial, Society for Industrial Mathematics, 2000.

[6] U. Trottenberg, C. Oosterlee, A. Schuller, Multigrid-2001, San Diego: Academic Press, 2001.

[7] A. Brandt, Barriers to Achieving Textbook Multigrid Efficiency (TME) in CFD, Institute for Computer Applications in Science and Engineering, NASA Langley Research Center, 1998.

[8] G. A. Gerolymos, I. Vallet, Mean-flow-multigrid for implicit Reynolds-stress-model computations, AIAA Journal 43 (9) (2005) 1887–1898.

[9] G. A. Gerolymos, I. Vallet, Implicit meanflow-multigrid algorithms for Reynolds stress model computation of 3-D anisotropy-driven and compressible flows, International Journal for Numerical Methods in Fluids 61 (2008) 185–219.

[10] R. C. Swanson, C. C. Rossow, An efficient flow solver with a transport equation for modeling turbulence, in: 19th AIAA Computational Fluid Dynamics, San-Antonio, Texas, 2009.

[11] J. Fassbender, Robust and efficient computation of turbulent flows around civil transport aircraft at flight Reynolds numbers, Aerospace Science and Technology 9 (8) (2005) 672–680.

[12] P. Walsh, T. Pulliam, The effect of turbulence model solution on viscous flow problems, in: 39th AIAA Aerospace Sciences Meeting & Exhibit, Reno, NV, 2001, aIAA - 2001-1018.

[13] T. Park, Multigrid method and low-reynolds-number k-ϵ model for turbulent recirculating flows, Numerical Heat Transfer, Part B: Fundamentals 36 (4) (1999) 433–456.

[14] P. Gerlinger, An evaluation of multigrid methods for the simulation of turbulent combustion, in: 17 th AIAA Computational Flow Dynamics Conference, 2005, pp. 1–14.

[15] M. Vazquez, M. Ravachol, F. Chalot, M. Mallet, The robustness issue on multigrid schemes applied to the Navier-Stokes equations for laminar and turbulent, incompressible and compressible flows, International Journal for Numerical Methods in Fluids 45 (5) (2004) 555–579.

[16] J. Yan, F. Thiele, L. Xue, A modified full multigrid algorithm for the Navier–Stokes equations, Computers and Fluids 36 (2) (2007) 445–454.

[17] Y. Mor-Yossef, Y. Levy, Unconditionally positive implicit procedure for two-equation turbulence models: Application to $k-\omega$ turbulence models, Journal of Computational Physics 220 (1) (2006) 88–108.

[18] C. Kok, Johan, Resolving the dependence on freestream values for the k-ω turbulence model, AIAA Journal 38 (7) (2000) 1292–1295.

[19] S. Wallin, A. Johansson, An explicit algebraic Reynolds stress model for incompressible and compressible turbulent flows, Journal of Fluid Mechanics 43 (2000) 89–132.

[20] P. Batten, M. A. Leschziner, U. C. Goldberg, Average-state Jacobians and implicit methods for compressible viscous and turbulent flows, Journal of Computational Physics 137 (1) (1997) 38–78.

[21] P. Jawahar, H. Kamath, A high-resolution procedure for Euler and Navier-Stokes computations on unstructured grids, Journal of Computational Physics 164 (1) (2000) 165–203.

[22] E. F. Toro, Riemann Solvers and Numerical Methods for Fluid Dynamics; A Practical Introduction (2nd edition), Springer-Verlag Berlin Heidelberg, 1999.

[23] A. Berman, R. J. Plemmons, Nonnegative matrices in the mathematical sciences, Computer Science and Applied Mathematics, Academic Press, Inc., New York, 1979.

[24] Y. Mor-Yossef, Y. Levy, The unconditionally positive-convergent implicit time integration scheme for two-equation turbulence models: Revisited, Computers & Fluids 38 (10) (2009) 1984–1994.

[25] A. Brandt, Multi-level adaptive solutions to boundary-value problems, Mathematics of Computations 31 (138) (1977) 333–390.

[26] U. Schumann, Realizability of Reynolds-stress turbulence models, Physics of Fluids 20 (1977) 721–725.

[27] S. Park, J. Kwon, Implementation of k-ω turbulence models in an implicit multigrid method, AIAA Journal 42 (2004) 1348–1357.

[28] D. Coles, A. J. Wadcock, Flying-hot-wire study of flow past an NACA 4412 airfoil at maximum lift, AIAA Journal 17 (4) (1979) 321–329.

[29] P. H. Cook, M. A. McDonald, M. C. P. Firmin, Aerofoil RAE2822-pressure distributions, boundary layer and wake measurements, Tech. Rep. AR 138, AGARD (1979).